



# Dendrimer-magnetic nanoparticles as multiple stimuli responsive and enzymatic drug delivery vehicle



Sudeshna Chandra<sup>a,1</sup>, Glen Noronha<sup>a</sup>, Sascha Dietrich<sup>b</sup>, Heinrich Lang<sup>b</sup>, Dhirendra Bahadur<sup>a,\*</sup>

<sup>a</sup> Metallurgical and Materials Science Department, Indian Institute of Technology Bombay, Powai, Mumbai, 400076, India

<sup>b</sup> Technische Universität Chemnitz, Institute of Chemistry, Straße der Nationen 62, d-09111 Chemnitz, Germany

## ARTICLE INFO

### Article history:

Received 31 July 2014

Received in revised form

17 October 2014

Accepted 18 October 2014

Available online 30 October 2014

### Keywords:

Magnetic nanoparticles

Dendrimers

Drug loading

Enzymatic release

Doxorubicin

## ABSTRACT

Two different chain lengths of (poly)ethylene glycol-PAMAM dendrimers namely, L6-PEG-PAMAM and S6-PEG-PAMAM with six end-grafted ethylene glycol ether-tentacles of type  $\text{CH}_2\text{CH}_2\text{C}(\text{O})(\text{CH}_2\text{CH}_2\text{O})_9\text{CH}_3$  and  $\text{CH}_2\text{CH}_2\text{C}(\text{O})(\text{CH}_2\text{CH}_2\text{O})_2\text{C}_2\text{H}_5$ , respectively, were synthesized. These dendrimers have multiple  $\sigma$ -donor capabilities and therefore, were used for stabilizing the magnetite ( $\text{Fe}_3\text{O}_4$ ) nanoparticles. Both the dendrimer-magnetic nanoparticles (L6-PEG-PAMAM-MNPs and S6-PEG-PAMAM-MNPs) were characterized by different spectroscopic and microstructural techniques. The nanoparticles were mesoporous and superparamagnetic and therefore, explored for their possible use in delivery of cancer drug, doxorubicin (DOX). In the developed drug delivery system, achieving high drug-loading efficiency with controllable release were the main challenges. The change in zeta potential and quenching of fluorescence intensity suggests chemical interaction between DOX and the nanoparticles. The loading efficiency was calculated to be over 95% with a sustained pH and temperature sensitive release. Further, enzyme cathepsin B has also been used to degrade the dendritic shell to trigger sustained drug release in the vicinity of tumor cells.

© 2014 Elsevier B.V. All rights reserved.

## 1. Introduction

Dendrimers are nano-sized highly ordered structure with numerous functional groups and internal cavities. These features make the dendrimers suitable for many biomedical applications like drug and gene delivery, biochemistry and nanomedicine [1]. Further, dendrimers are also considered as nonviral synthetic vectors due to its biocompatibility, simplicity of use, and easy synthesis as compared to viral vectors which has inherent risk for clinical use [2].

Magnetic nanoparticles (MNPs), on the other hand, have proven applications in hyperthermia, magnetic resonance imaging contrast agent, targeted drug and gene delivery, tissue engineering, cell tracking, biosensing and bioseparation [3]. When functionalized with macromolecules, MNPs form distinct particulate systems that can pass through cellular barriers and offer organ-specific therapeutic and diagnostic tools [4]. Surface chemistry plays an important role in regulating the physiochemical characteristics of MNPs, viz., size, solubility, state of dispersion and

magnetization and also influences the fate of the MNPs in the biological system. MNPs coated with dendrimers can have better prospective in terms of surface charge, functionality, and reactivity as well as enhanced stability and dispersibility in solution [5]. Nanotechnology researchers have combined these two very effective materials to produce a nanoscale construct that can be effectively used for various biological applications.

Targeted drug-delivery systems can effectively convey drugs to the desired site of action, increase patient compliance, extend the product life cycle, and reduce healthcare costs [6]. However, in the current scenario, targeted drug delivery is a bottleneck since most of the drugs have low solubility, rapid excretion and high toxicity. They are also limited by untargeted biodistribution and non-specific delivery, *in vivo* degradation and short circulating half-lives [7]. All these drawbacks can be addressed by introducing polyethylene glycol groups (PEGylation) in the nanosystems. After PEGylation, many drugs have been found to attain increased solubility, improved pharmacokinetics and targeting [8].

The motivation for the study is to combine the functions of longevity (PEGylation in dendrimer), targetability (use of MNP to assist in magnetic guidance to tumor site) and stimuli sensitivity (pH, temperature) in addition to leveraging the tumor micro-environment (acidic pH, over-expression of enzymes promoting degradation) to design an efficient, minimally toxic drug delivery

\* Corresponding author.

E-mail address: [dhiren@iitb.ac.in](mailto:dhiren@iitb.ac.in) (D. Bahadur).

<sup>1</sup> present address: Department of Chemical Sciences, School of Science, NMIMS University, Mumbai, 400056, India.

system. It was also aimed to fabricate the system in such a way that it would release maximum payload at the tumor site and minimum during circulation.

The present study aims to synthesize dendrimer based MNPs wherein the dendrimer stabilizes the nanoparticles and provides functional groups for attachment of drug molecules. Thorough characterization of the functionalized MNPs has been performed to gauge particle size distribution, surface area, porosity and magnetic properties. Loading of doxorubicin and their subsequent release in acidic, hyperthermic and enzymatic (cathepsin B) environment has also been investigated.

## 2. Experimental

### 2.1. Materials used

Ferric chloride hexahydrate ( $\text{FeCl}_3 \cdot 6\text{H}_2\text{O}$ ), ferrous chloride tetrahydrate ( $\text{FeCl}_2 \cdot 4\text{H}_2\text{O}$ ), sodium hydroxide and doxorubicin hydrochloride were received from Sigma Aldrich, USA. All other chemicals were of analytical grade and used as received.

The poly(ethyleneglycol)-poly(amidoamine) dendrimers were synthesized [9,10] and used to stabilize and functionalize the magnetic nanoparticles. One of the dendrimers had 6 long dendritic arms (L6-PEG-PAMAM) and the other dendrimer had 6 comparatively short arms (S6-PEG-PAMAM) (Fig. 1).

The MNPs were prepared by the conventional co-precipitation technique with 2:1 M ratio of  $\text{Fe}^{3+}/\text{Fe}^{2+}$ . Typically, 6 g  $\text{FeCl}_3 \cdot 6\text{H}_2\text{O}$  and 2.1 g  $\text{FeCl}_2 \cdot 4\text{H}_2\text{O}$  in 80 mL deionised water was stirred in a five-necked flask under inert atmosphere for 30–45 min until a temperature of 80 °C was reached. To this solution, 20 mL of 5 M NaOH was added drop by drop, following which the solution turned from orange to black. The reaction mixture was then vigorously stirred at 1000 rpm for 1 h. 10 mL dendrimer solution (1 mg/mL concentration) was added and the refluxing was continued for another 30 min, after which the system was cooled to room temperature. The solution was washed alternatively with deionised water and ethanol for 3–4 times. A permanent magnet was then used to separate the dendrimer stabilized magnetic nanoparticles. The magnetically separated nanoparticles are named as L6-PEG-PAMAM-MNPs and S6-PEG-PAMAM-MNPs.

### 2.2. Characterization techniques

The phase purity and identification of the MNPs were done by X-ray diffraction (XRD) with PanAnalytical X-Pert diffractometer using a monochromatised X-ray beam with nickel-filtered  $\text{Cu-K}\alpha$  radiation at 4°/min scan rate. Fourier transform infrared (FT-IR) spectra were obtained using a Jasco, FT-IR 300E spectrometer with a resolution of 4  $\text{cm}^{-1}$ . The TEM micrographs were observed by JEOL JEM 2100 for particle size determination. The specific surface area, pore volume and pore size distribution of the nanoparticles were measured by ASAP 2020 Micromeritics instrument. Magnetic properties of MNPs were studied using Vibrating Sample Magnetometer Model: 7410, Lake Shore Cryotronics Inc., U.S.A.

### 2.3. Drug loading and release

The anticancer agent, doxorubicin hydrochloride (DOX) was used to study the drug loading and release efficiency of the dendrimer-MNPs. Fluorescence spectroscopy was used to investigate the interaction of DOX with L6- and S6-PEG-PAMAM-MNPs.

A typical drug loading method is as follows: The aqueous dispersion of varying amounts of L6- and S6-PEG-PAMAM-MNPs (1, 2, 4, 6 and 8 mg/mL from a stock suspension) were added to a fixed amount of DOX solution (50  $\mu\text{g}$ ) and incubated by shaking at ambient temperature for 24 h. The loading percentages for different concentrations of nanoparticles were calculated by comparing the fluorescence peak intensities of the supernatant of the DOX loaded nanoparticles against the fluorescence spectrum of pure DOX solution. The standard curve of DOX solution was prepared by recording the individual fluorescence intensities under similar conditions using Cary Eclipse fluorescence spectrophotometer ( $R^2=0.998$ ) [10,11]. The loading efficiency (w/w%) was calculated using the following relation:

$$\text{Loading efficiency (\%)} = \frac{I_{\text{DOX}} - I_s}{I_{\text{DOX}}} \times 100$$

where,  $I_{\text{DOX}}$  is the fluorescence intensity of pure DOX solution and  $I_s$  the fluorescence intensity of the supernatant solution. The loading interactions were evaluated at  $\lambda_{\text{ex}}=490$  nm and  $\lambda_{\text{em}}=590$  nm for DOX.

For studying the drug release profile, various external stimuli like change in pH, temperature and enzymatic degradation was used. The drug release under the influence of pH was carried out in a reservoir-sink condition. Typically, 4 mg of drug loaded

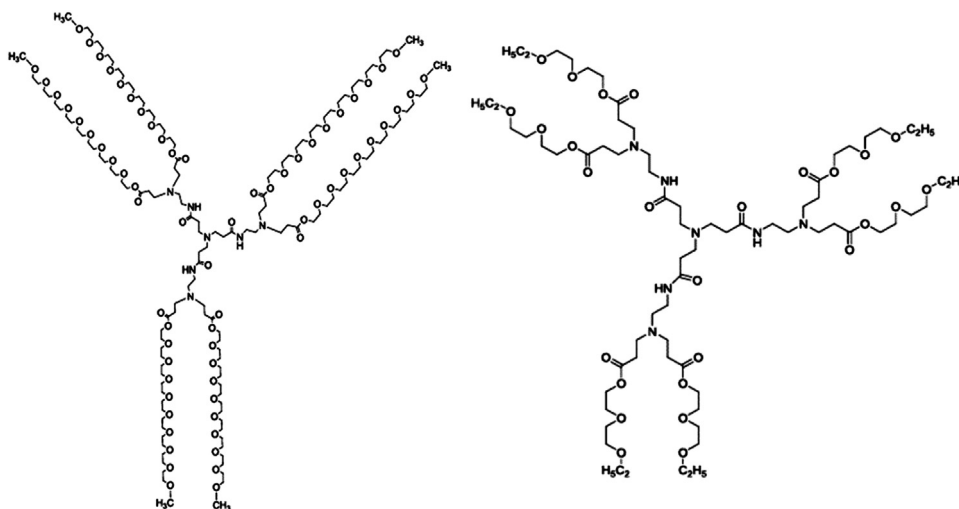


Fig. 1. Structure of dendrimers: (a) long branch or L6-PEG-PAMAM and (b) short branch or S6-PEG-PAMAM.

nanoparticles were dissolved separately in 1 mL of acetate buffer (pH 4.3) and PBS (pH 7.4) and put into a dialysis bag. The dialysis was performed against 20 mL of PBS (pH 7.4) under continuous magnetic stirring at room temperature. 2 mL of the external medium was collected at fixed interval of time and replaced with fresh PBS to maintain the sink conditions. The amount of DOX released was determined by recording the fluorescence intensity curves at  $\lambda_{\text{ex}}=470$  nm and  $\lambda_{\text{em}}=590 \pm 5$  nm and comparing the standard plot prepared under similar condition [11].

Drug release experiments were also performed to study the temperature-sensitive release profile at human body temperature (37 °C) and hyperthermia temperature ( $43 \pm 2$  °C). Similar protocols were used for sample collection at pre-determined time intervals and measurement of fluorescence intensities.

### 3. Enzymatic release

Enzymatic release was determined by adapting the method of Chu et al. [12]. Typically, 1 mL of bovine cathepsin B (100  $\mu\text{g}/\text{mL}$  concentration) was added to activation buffer consisting of 21.2 mg EDTA in 5 mL deionised water and incubated at 37 °C for 15 min. The reaction buffer was prepared by adding 29.8 mg of EDTA and 2.5 mL of acetate (1 M) to 97.5 mL of water and warmed to 37 °C. Finally, 2 mL enzyme solution and 1 mL of drug loaded nanoparticles (10 mg) were added to 97 mL of reaction buffer in a flat-bottomed flask and the system was incubated at 37 °C accompanied with simultaneous shaking. At regular time intervals, 2 mL of the reaction solution was extracted with the help of syringes. The fluorescence spectra of the supernatants were immediately recorded.

### 4. Results and discussion

Fig. 2 shows the FTIR spectra of the pure L6-PEG-PAMAM dendrimer and L6-PEG-PAMAM-MNPs. The absorption bands of the pure dendrimer are well resolved but those of L6-PEG-PAMAM-MNPs are rather broad and few. The peak at  $1728\text{ cm}^{-1}$  and  $1660\text{ cm}^{-1}$  due to the C=O (asym. str.) of the ester and amide bonds, respectively, shifts to lower wave numbers in L6-PEG-PAMAM-MNPs revealing the binding nature of the dendrimer to the  $\text{Fe}_3\text{O}_4$  nanoparticles through CO functionality. Possibly, the surface

bonding involves a dative bond from the electron lone pair of the C-atom in CO to the Fe-atom and  $\pi$  back-donation of electron density from the metal to carbonyl functionality. This causes weakening of the carbonyl bond, which shifts the stretching frequencies to lower values [13].

The broad band at  $3200\text{ cm}^{-1}$  is due to the O–H and N–H stretching vibrations, while the ones at  $2880\text{ cm}^{-1}$  and  $2830\text{ cm}^{-1}$  corresponds to the asymmetric and symmetric  $\text{CH}_2$  stretching modes. The absorption at  $1352\text{ cm}^{-1}$  is assigned to the C–N stretching of the amine, while the series of bands from  $1245\text{ cm}^{-1}$  to  $955\text{ cm}^{-1}$  can be attributed to the  $\text{CH}_2$  wagging and twisting, as also the C–O–C stretching vibrations [14,15]. The reduced intensity of these bands in L6-PEG-PAMAM-MNPs suggests that the  $\text{Fe}_3\text{O}_4$  nanoparticles may be bonded to the ethylene glycol arms of the dendrimer as well. The strong absorption band at  $588\text{ cm}^{-1}$  can be ascribed to the Fe–O stretching vibrational mode of  $\text{Fe}_3\text{O}_4$ . Similar observations were made in case of S6-PEG-PAMAM-MNPs.

The XRD pattern of L6- and S6-PEG-PAMAM-MNPs show 6 diffraction peaks: (220), (311), (400), (422), (511) and (440) at  $30.4^\circ$ ,  $35.6^\circ$ ,  $43.5^\circ$ ,  $53.3^\circ$ ,  $57.2^\circ$ ,  $62.8^\circ$  and  $30.4^\circ$ ,  $35.7^\circ$ ,  $43.4^\circ$ ,  $53.9^\circ$ ,  $57.4^\circ$ ,  $62.8^\circ$   $2\theta$ , respectively. This indicates the formation of a single-phase  $\text{Fe}_3\text{O}_4$  inverse spinel structure in both the MNPs. The presence of sharp and intense peaks confirms the formation of highly crystalline nanoparticles.

The TEM image of L6-PEG-PAMAM-MNPs shows spherical and irregular shaped nanoparticles. The histogram of size distribution of the MNPs (Fig. 3) showed that the mean size of the nanoparticles are  $\sim 9.6$  nm with a standard deviation  $\pm 0.13$  nm. The particle size data is based on the image analysis of more than 100 well dispersed nanoparticles. Inset (a) of Fig. 3 reveals the electron diffraction ring patterns with  $d$ -spacings of 2.93, 2.52, 2.08, 1.71, 1.61, 1.48 Å, which match the standard body centered cubic spinel structure (JCPDS card No. 88-0315). Inset (b) of Fig. 3 shows the HRTEM image L6-PEG-PAMAM-MNPs crystallite with  $d$ -spacing of 2.93 Å which corresponds to the (220) plane of  $\text{Fe}_3\text{O}_4$ . The TEM image of S6-PEG-PAMAM-MNPs also shows spherical and irregular shaped particles of  $\sim 7.0 \pm 0.04$  nm.

Fig. 4 shows the field dependent magnetization of dendrimer-MNPs at 300 K. It can be seen that the saturation magnetization at 20,000 G for L6- and S6-PEG-PAMAM-MNPs is 45.9 and 41.6 emu/g, respectively. In addition, both samples exhibited typical superparamagnetic behavior which makes the nanoparticles useful for magnetic drug targeting.

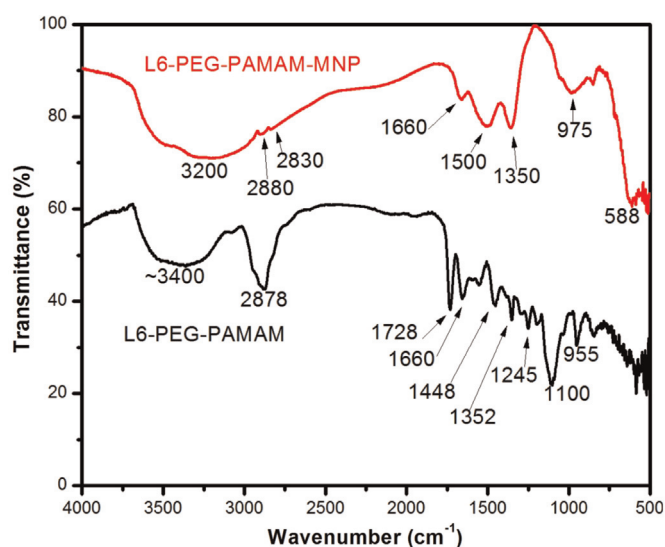


Fig. 2. FTIR spectra of pure L6-PEG-PAMAM dendrimer and L6-PEG-PAMAM-functionalised MNPs.

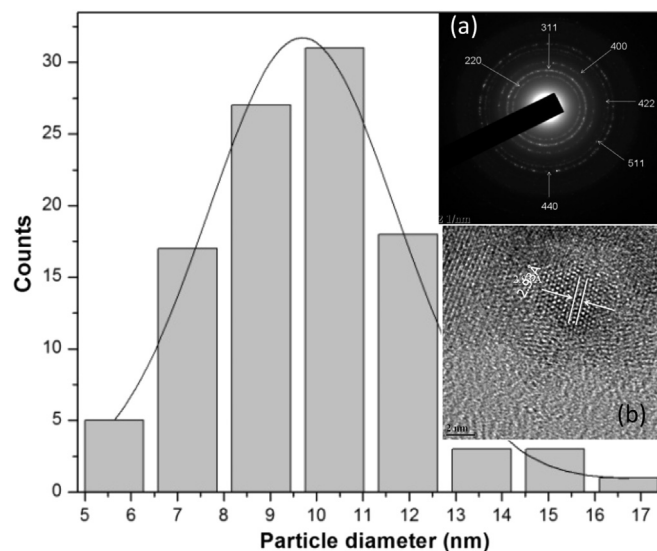


Fig. 3. Histogram depicting particle size distribution of L6-PEG-PAMAM-MNPs; Inset (a) electron diffraction pattern and (b) HR-TEM image.

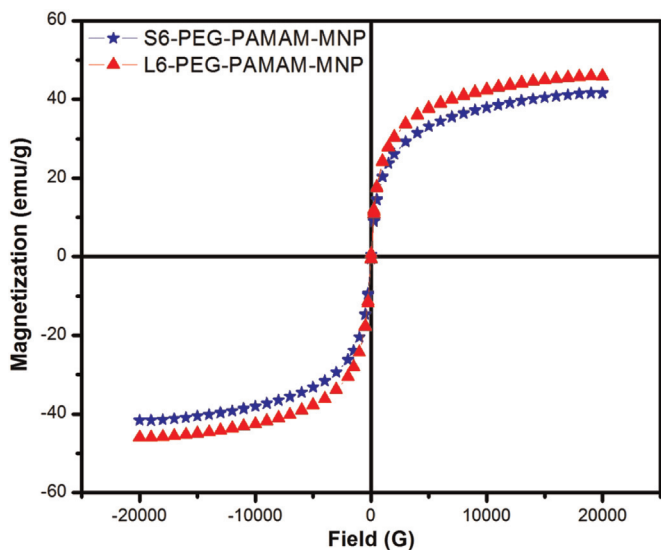


Fig. 4. Field dependent magnetization plot of L6- and S6-PEG-PAMAM-MNPs at 300 K.

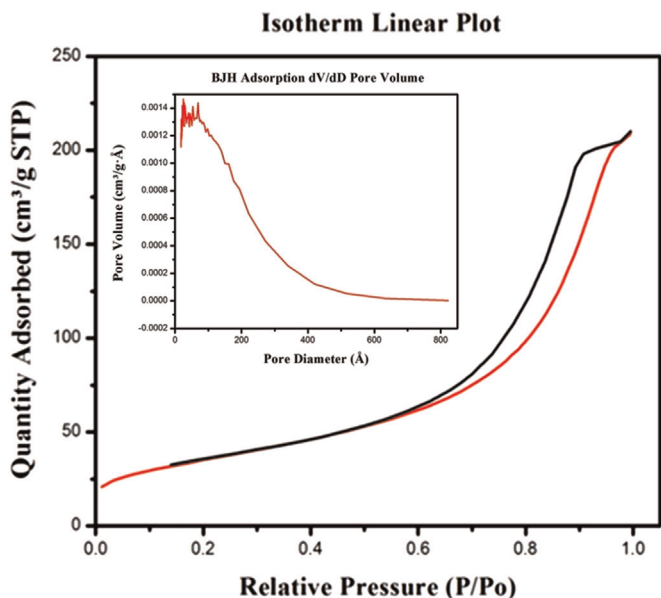


Fig. 5. N<sub>2</sub> adsorption-desorption isotherms and pore size distribution (inset) for L6-PEG-PAMAM-MNPs.

The N<sub>2</sub> adsorption-desorption isotherm and pore size distribution for L6-PEG-PAMAM-MNPs are shown in Fig. 5. The increase in the N<sub>2</sub> uptake at higher relative pressure ( $P/P_o > 0.5$ ) for the MNPs was due to adsorption in mesopores and the generated N<sub>2</sub> isotherms are close to Type IV [16,17] with an evident hysteresis loop at relative pressure of 0.5 and above. In the isotherm there is a horizontal region of nearly flat adsorption within the region of relative pressure of 0.2–0.5 followed by a sudden rise. The hysteresis loop for the nanoparticles can be assigned to the H1 type

Table 1  
Textural analyses of the nanoparticles.

Samples	BET surface area (m <sup>2</sup> /g)	Total pore volume (cm <sup>3</sup> /g)	Average pore diameter (Å)
L6-PEG-PAMAM-MNPs	127	0.316	93
S6-PEG-PAMAM-MNPs	138	0.393	109

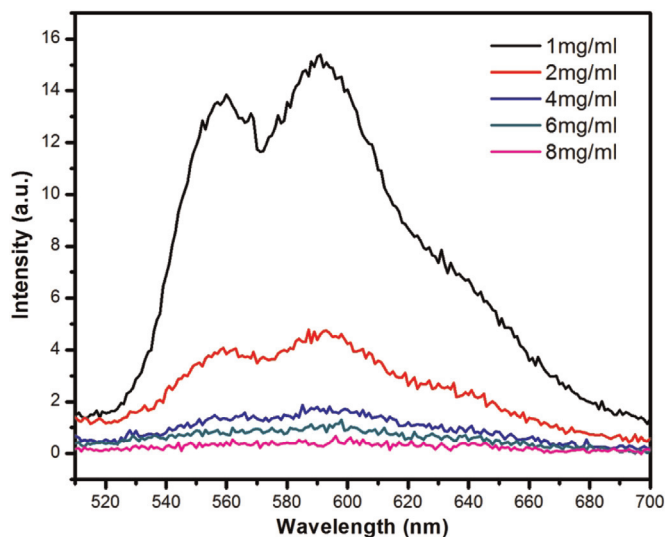


Fig. 6. Fluorescence spectra of supernatants of DOX reacted with different amounts of L6-PEG-PAMAM-MNPs.

[16], indicating the presence of agglomerates or compacts of approximately uniform spheres in a fairly regular array. The textural analyses of the nanoparticles are tabulated in Table 1.

### 5. Drug loading and release

The interaction of DOX molecules with L6- and S6-PEG-PAMAM-MNPs is evident from the predominant quenching of DOX fluorescence in presence of nanoparticles (Figs. 6 and 7).

The decrease in the fluorescence intensity of DOX with increase in the concentration of PEG-PAMAM-MNPs was obvious due to the loading of DOX onto the nanoparticles [11]. The loading efficiency is strongly dependent on the particles to DOX ratio. The obtained high loading efficiency (~98.7%, w/w) is due to the electrostatic interaction of the between positively charged DOX molecules and negatively charged carboxyl and ethylene glycol moieties of the dendrimer-MNPs. The detection limit for DOX loading efficiency measurements was found to be approximately 2 µg/mL.

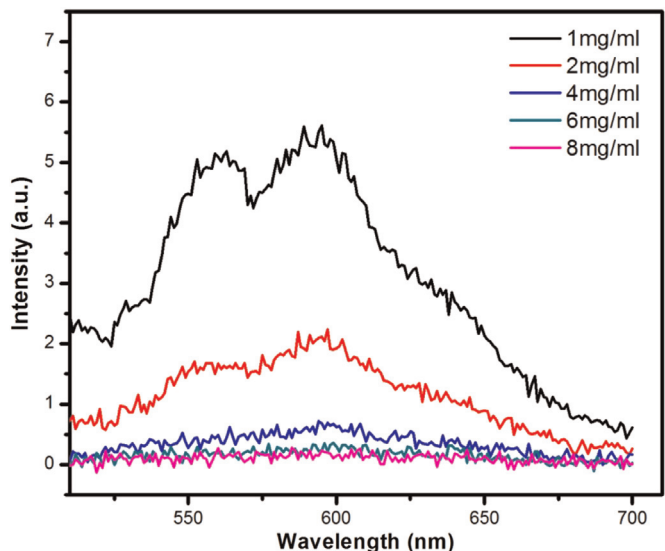


Fig. 7. Fluorescence spectra of supernatants of DOX reacted with different amounts of S6-PEG-PAMAM-MNPs.

The zeta-potential measurements of L6- and S6-PEG-PAMAM-MNPs at different pH indicate bounding of  $\text{Fe}_3\text{O}_4$  with the PEG-PAMAM dendrimers. The high negative values of zeta-potential for the L6- and S6-PEG-PAMAM-MNPs indicates that the surface of the nanoparticles are surrounded by the negatively charged carboxyl and ethylene glycol groups of the dendrimers.

The change in values of zeta-potential for unloaded and drug loaded nanoparticles indicate loading of doxorubicin onto dendritic arena [18]. The observed increase in potential of the entire system is due to the loading of the positively charged DOX was loaded onto the dendrimer-nanoparticles. This indicates an electrostatic nanoparticles–drug interaction.

## 6. pH- and temperature-dependent drug release

Fig. 8 shows the drug release profile of DOX-loaded L6- and S6-PEG-PAMAM-MNPs in cell mimicking environment.

The drug loaded L6-PEG-PAMAM-MNPs released  $\sim 38\%$  of loaded DOX in acetate buffer (pH 4.3) against PBS (pH 7.3) after 50 h. However, only  $\sim 25\%$  DOX was released in the PBS against PBS (pH 7.4) solution. In case of S6-PEG-PAMAM-MNPs, the drug release was  $\sim 25$  and  $20\%$  in acetate buffer (pH 4.3) and PBS (pH 7.4), respectively after 70 h. The weakening of the electrostatic

interactions between DOX and the partially neutralized carboxyl and ethylene glycol groups on the nanoparticles resulted in the release of DOX [19]. Since weakening of the electrostatic interactions is a slower process, a sustained release is achieved over a period of 50 and 70 h in L6-PEG-PAMAM-MNPs and S6-PEG-PAMAM-MNPs, respectively.

*In vitro* release profiles of DOX from L6-PEG-PAMAM-MNPs in PBS (pH 7.4) as a function of time at 37 and 43 °C was carried out. It was noted that at the physiological temperature (37 °C), the release is about  $\sim 20\%$  over a period up to 19 h, while it goes up to about  $\sim 38\%$  at 43 °C, a possible hyperthermic temperature. With respect to S6-PEG-PAMAM-MNPs, the cumulative release stood at  $\sim 30\%$  at 43 °C, and  $\sim 25\%$  at 37 °C. Overall, rapid release took place in the initial 10–15 h, followed by gradual release thereafter.

## 7. Enzymatic release of DOX

As a proof of concept, we studied the enzymatic breakdown of the nanoparticles with Cathepsin B. Fig. 9 shows the release profiles of DOX from the nanoparticles in the presence of Cathepsin B. The initial release of  $\sim 20\%$  can be attributed to hydrolysis of the dendritic system due to dilution effect. Within 24 h, almost 40% of the loaded doxorubicin is released. This release is higher than both pH and temperature dependent release observed earlier. It is also

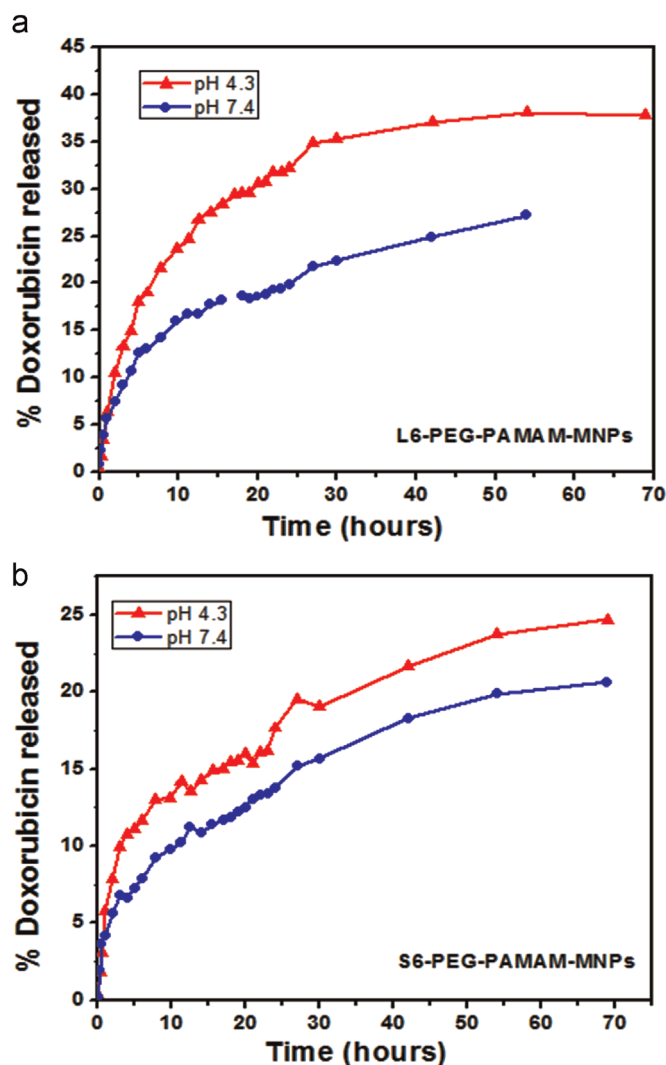


Fig. 8. pH-dependent release of DOX from (a) L6-PEG-PAMAM-MNPs and (b) S6-PEG-PAMAM-MNPs.

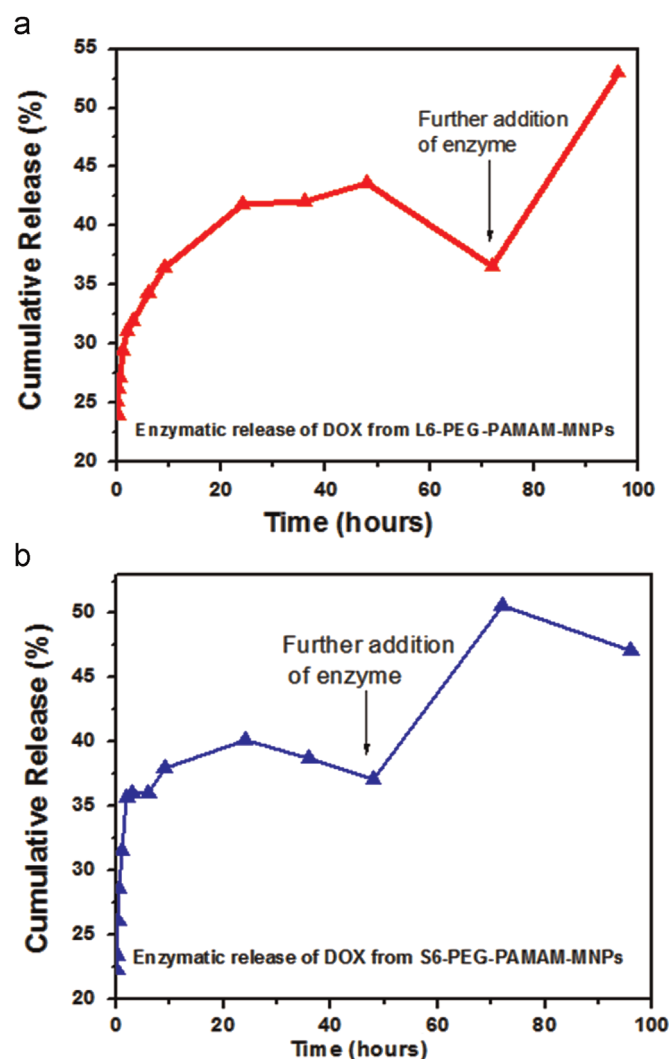


Fig. 9. Cathepsin B-mediated release of DOX from (a) L6-PEG-PAMAM-MNPs and (b) S6-PEG-PAMAM-MNPs.

observed that the enzymatic activity decreases after 24 h, indicated by the flattening of the cumulative release profile. Upon further addition of activated enzyme solution, a sharp burst release was observed. Thus, in conditions simulating the extra-cellular matrix or lysosomes of target cells, it is inferred that the enzyme degrades the carrier and enhances the drug release.

It has been observed that for a fixed time frame, the quantity of drug released is higher at tumor microenvironment as compared to neutral pH (blood environment). It is also higher at higher temperature as compared to body lower temperature. Additionally, the presence of enzymes in the extracellular region of the tumor cells promotes faster release rate by degrading the carrier. Thus, the combined effect of the acidic tumor microenvironment containing enzymes, coupled with the use of temperature as a stimulus would result in a faster and higher release of drug, as compared with the effects of each condition individually.

## 8. Conclusions

Magnetic nanoparticles (MNPs) were stabilized and functionalized with L6-PEG-PAMAM and S6-PEG-PAMAM dendrimers. The crystalline spherical nanoparticles were superparamagnetic with average particle size of  $\sim 10$  nm. Surface area and pore diameters of the MNPs were found to be very promising for use as drug carrier. The concept of applying a stimulus (*via* pH or temperature change) followed by enzymatic breakdown of the nano-carrier is a new approach to develop a controlled drug release system wherein both targeted and sustained release of drug is achieved. The dendrimer-magnetic nanoparticles may be looked upon as high-efficiency drug delivery system with the potential to achieve magnetic drug targeting and magnetic hyperthermia.

## Acknowledgments

Author acknowledges Alexander-von-Humboldt Foundation (AvH), Germany, Department of Electronics and Information Technology (DEIT), and Nanomission of DST, Govt. of India.

## References

- [1] B. Pan, D. Cui, Y. Sheng, C. Ozkan, F. Gao, R. He, Q. Li, P. Xu, T. Huang, Dendrimer-modified magnetic nanoparticles enhance efficiency of gene delivery system, *Cancer Res.* 67 (2007) 8156–8163.
- [2] I.J. Majoros, T.P. Thomas, C.B. Mehta, J.R. Baker, Poly(amidoamine) dendrimer-based multifunctional engineered nanodevice for cancer therapy, *J. Med. Chem.* 48 (2005) 5892–5899.
- [3] V.I. Shubayev, T.R. Pisanic, S. Jin, Magnetic nanoparticles for theragnostics, *Adv. Drug Deliv. Rev.* 61 (2009) 467–477.
- [4] J.R. McCarthy, K.A. Kelly, E.Y. Sun, R. Weissleder, Targeted delivery of multifunctional magnetic nanoparticles, *Nanomedicine* 2 (2007) 153–167.
- [5] B. Pan, F. Gao, L. Ao, Investigation of interactions between dendrimer-coated magnetite nanoparticles and bovine serum albumin, *J. Magn. Magn. Mater.* 293 (2005) 252–258.
- [6] S. Parveen, S.K. Sahoo, Nanomedicine: clinical applications of polyethylene glycol conjugated proteins and drugs, *Clin. Pharmacokinet.* 45 (2006) 965–988.
- [7] G. Orive, R.M. Hernandez, A. Rodriguez Gascon, A. Dominguez-Gil, J.L. Pedraz, Drug delivery in biotechnology: present and future, *Curr. Opin. Biotechnol.* 14 (2003) 659–664.
- [8] F.M. Veronese, G. Pasut, PEGylation, successful approach to drug delivery, *Drug Discov. Today* 10 (2005) 1451–1458.
- [9] S. Dietrich, S. Schulze, M. Hietschold, H. Lang, Au nanoparticles stabilized by PEGylated low generation PAMAM dendrimers: design, characterization and properties, *J. Colloid Interface Sci.* 359 (2011) 454–460.
- [10] S. Dietrich, S. Chandra, C. Georgi, S. Thomas, D. Makarov, S. Schulze, M. Hietschold, M. Albrecht, D. Bahadur, H. Lang, Design, characterization and magnetic properties of  $\text{Fe}_3\text{O}_4$  nanoparticles arrays coated with PEGylated dendrimers, *Mater. Chem. Phys.* 132 (2012) 292–299.
- [11] S. Nigam, K.C. Barrick, D. Bahadur, Development of citrate-stabilized  $\text{Fe}_3\text{O}_4$  nanoparticles: conjugation and release of doxorubicin for therapeutic applications, *J. Magn. Magn. Mater.* 323 (2011) 237–243.
- [12] D.S.H. Chu, R.N. Johnson, S.H. Pun, Cathepsin B-sensitive polymers for compartment-specific degradation and nucleic acid release, *J. Control. Release* 157 (2012) 445–454.
- [13] F. Zaeraa, New advances in the use of infrared absorption spectroscopy for the characterization of heterogeneous catalytic reactions, *Chem. Soc. Rev.* 43 (2014) 7624–7663.
- [14] J. Zhang, R.D.K. Mishra, Magnetic drug-targeting carrier encapsulated with thermosensitive smart polymer: core-shell nanoparticle carrier and drug release response, *Acta Biomater.* 3 (2007) 838–850.
- [15] T.K. Jain, M.A. Morales, S.K. Sahoo, D.L. Leslie-Pelecky, V. Labhasetwar, Iron oxide nanoparticles for sustained delivery of anticancer agents, *Mol. Pharm.* 2 (2005) 194–205.
- [16] K. Kaneko, Determination of pore size and pore size distribution: adsorbents and catalysts, *J. Membr. Sci.* 96 (1994) 59–89.
- [17] J.C. Groen, L.A.A. Peffer, J.P. Ramirez, Pore size determination in modified micro- and mesoporous materials. Pitfalls and limitations in gas adsorption data analysis, *Microporous Mesoporous Mater.* 60 (2003) 1–17.
- [18] S. Chandra, S. Dietrich, H. Lang, D. Bahadur, Dendrimer-doxorubicin conjugate for enhanced therapeutic effects for cancer, *J. Mater. Chem.* 21 (2011) 5729–5737.
- [19] T. Etrych, P. Chytil, M. Jelinkova, B. Rihova, K. Ulbrich, Synthesis of HPMA copolymers containing doxorubicin bound via a hydrazone linkage. Effect of spacer on drug release and *in vitro* cytotoxicity, *Macromol. Biosci.* 2 (2002) 43–52.